Saha *et al.*
Protection and Control of Modern Power Systems (2022) 7:47
https://doi.org/10.1186/s41601-022-00266-7

Protection and Control of Modern Power Systems

ORIGINAL RESEARCH Open Access

Cascade controller based modeling of a four area thermal: gas AGC system with dependency of wind turbine generator and PEVs under restructured environment

Debdeep Saha[1*], Lalit Chandra Saikia[2] and Asadur Rahman[3]

Abstract

This paper investigates automatic generation control (AGC) of a realistic hybrid four-control area system with a distinct arrangement of thermal units, gas units and additional power generation. A proportional-integral-double derivative cascaded with proportional-integral (PIDD-PI) controller is employed as secondary controller in each control area for robust restructured AGC considering bilateral transactions and contract violations. The Harris Hawks algorithm is used to determine the optimal controller gains and system parameters under several scenarios. Electric vehicle (EV) aggregators are employed in each area to participate fully along with thermal and gas units to compensate for the unscheduled system demand in the local area. A comparison of non-cascaded controllers such as PI-PD, PD-PID and the proposed PIDD-PI proves the superiority of the last. The effect of the decline in inertia is closely examined because of the sudden outage of a generating unit while at the same time considering the change in area frequency response characteristics and area control error. EV fleets make significant contributions to improving the system dynamics during system inertia loss. The use of EVs in the presence of a wind energy-supported grid can provide a stable efficacy to the power grid. Numerous simulations with higher load demands, stochastic communication delays in presence of the WTG plant, and violations in system loadings and changes in gas turbine time constants in the absence of WTG demonstrate the robustness of the proposed control approach.

Keywords: Automatic generation control, Cascade controller, Electric vehicle, Harris Hawks algorithm, Wind turbine generator

1 Introduction

A properly designed power system can deal with sudden load changes and system frequency fluctuations. It should be able to regulate system voltage and frequency within prescribed operating limits to offer satisfactory power quality [1]. However, deviations from the normal operating condition can occur because of load change and this can result in frequency and tie-power deviations from scheduled standard deviations that may be undesirable [2]. Presently, the power industry maintains vertically integrated utility (VIU) structure which constitutes generation (GENCO), transmission (TRANSCO) and distribution (DISCO) companies. One VIU always maintains the transmission voltage level when interconnected to other VIUs [3]. In the AGC regime, every particular service unit operates in its regulated region and can identify its area control error by adopting the tie-line bias control concept [4]. The open Market Scenario is a collective effort of well-designed market policies and economic benefits which leads to good quality of service. The independent entities of GENCOs, TRANSCOs, and

*Correspondence: saha_debdeep_RS@yahoo.com

[1] Department of Electrical Engineering, Indian Institute of Engineering Science and Technology Shibpur, Shibpur, West Bengal, India
Full list of author information is available at the end of the article

DISCOs play a discrete function in the AGC sphere and, need to be modeled differently [5].

Many researchers have contributed toward designing a multi-area AGC model in the restructured regime. Rahman et al. [6] maintained the frequency change in a grid-associated multi-control area power system comprising hydro and thermal units under an open market scenario. AGC operation of a multi-area multi-unit thermal system is characterized by cost-based analysis which is subjected to various changes in load and contingencies [7]. Also, Shiva and Mukherjee [8] extended the restructured AGC study to five area systems which comprise conventional units with realistic constraints consideration like generation limiting (GRC), governor dead zone (GDB) and signal delay. Morsali et al. [9] designed a thyristor-controlled series capacitor to damp out the oscillations in a conventional system with GRC, GDB and delay.

Climate change, energy reliability and security needs, and environmental pollution have promoted the need for more penetration of renewable energy [10]. There has been a growing popularity of wind generation although wind generations, intermittent and hence no fixed generation can be ensured. Thus conventional plants have to provide the additional reserve for the undispatchable wind generation [11–13]. Also, there has to be a limit on the integration of renewable sources in the grid because of supply-generation mismatch, voltage swings and frequent instability of the grid [14, 15]. With wind power integration, the overall inertia of the system decreases because of intermittency and an increase in the regulation constant [16]. An investigation was carried out at Great Britain's electricity network to analyze the challenges of governor control with a developed stochastic modeling tool [17] while here might be compromise of the frequency regulation of the power system with high wind energy integration [18].

The presence of controllable loads or distributed energy resources such as electric vehicles can offer frequency support thereby increasing the inertia of a renewable integrated energy system. This notion has established a concept of plug-in transportation such as plug-in electric-powered vehicles or hybrid vehicles whose reliance is on fossil fuels and be able to interface to the grid for charging and discharging [19]. Debbarma and Dutta [20] introduced electric vehicles integrated with other traditional sources such as hydro, thermal, and gas turbine units in LFC studies under an open market scenario while [21] introduced a new participation factor to implement the extent of participation of plug in vehicles for primary control to improve the frequency characteristics. Similar strategies with V2G have been designed for secondary control of integrated power networks [22]. A smart charging method for electric vehicles based on the V2G strategy is proposed for secondary frequency control to remove the unbalance between demand and generation [23]. Singh et al. [24] showed V2G feasibilities in modelling a characteristic distribution network of a metropolitan area to meet maximum demand along with decreased voltage sag. Nguyen et al. [16] integrated the concept of Certainty Equivalent and Adaptive Control and an agenda to be participated by the customer for coordinating both the charging and discharging of EVs.

Most of the literature on AGC is mainly focused on the design of non-cascade controllers such as integral [23], proportional-integral-derivative [7, 13], three-degree-of-freedom proportional-integral-derivative [6], and fractional-order proportional-integral-derivative [20]. These controllers have been successfully used as secondary controllers in conventional systems with two [16], three [7] and five areas [8]. Johnson Michael and Moradi Mohammad [25] used a tuned PID controller for non-linear cascade control systems, while [26] analyzed process control data collected from one shot industry using two PID controllers. In non-cascade controllers, the number of fine-tuning knobs is fewer than those in cascade controllers. The presence of more tuning knobs in the controller can be advantageous for obtaining better results. Dash et al. [27] explored the performance of PI-PD and PD-PID [28] controllers in four and three area thermal systems respectively by subjecting the system to various disturbances and uncertainties. However, the feasibility and performance of the cascade controller have not been evaluated in multi-area open market AGC systems consisting of electric vehicles and wind generation. Thus, the application of cascade controllers in restructured AGC needs to be studied.

The main difficulty concerned with any sort of controller is the selection of the optimal parameters that reduce the changes and ensure zero area control error (ACE). With the advent of computation, optimizing multiple data is no longer a problem. Most research is now carried out with a touch of optimization algorithms [6–8]. The reason for this is that the entire research problem in reality is highly non-linear, and it is necessary to find the optimum solution. Several minimizations or maximization algorithms such as novel genetic algorithm, powerful particle swarm optimization [9], biogeography based optimization [7], quasi oppositional harmony search [9], have been successfully applied in two-area, three area restructured multi-area multi-source systems for tuning gains of 3DOF-PID [6] FOPID [20] controllers. A meta-heuristic algorithm

based on a group of hawks trying to chase its targeted rabbit with its features of predator birds for tracing, encircling, flushing out and capturing the potential animal (rabbit) is known as the Harris Hawks Algorithm [29]. In the algorithm, the leader of the hawks attacks the prey. If it is not successful because of the dynamic nature and fast escape of the prey switching strategies are followed by other hawks in the group to hit the escaped prey until seized. The flowchart and steps can be found in [30, 31]. With puzzling and exhausting of the escaped prey, birds can find the targeted rabbit. This is a promising advantage of the combined strategy. Thus, the Harris Hawk Optimization (HHO) maintains the balance in the exploratory and exploitative phases.

The objectives of this paper are as follows:

1. To develop a four area hybrid AGC model of a realistic power system with six GENCOs and six DISCOS having thermal and gas generating units integrated with wind turbine generation (WTG) in all control areas.
2. To compare the performance of PID, PI-PD, PD-PID and PIDD-PI controllers as secondary controllers during bilateral transactions and determine the best.
3. To facilitate the test system with EV aggregators and evaluate the effect of discharged EV aggregators in meeting uncontracted load demand using HHO optimized best controller obtained in (2).
4. To demonstrate the effect of a decline in inertia for the system considered in (3) due to sudden outage of a generating unit in an area considering the change in area frequency response characteristics and area control error. To investigate the significance of EV aggregators for the above scenario.

2 Power system framework

Figure 1 shows the representation diagram of four-area multi-unit grid-connected systems in an open market environment. Each of Area 1 and 4 are employed with two thermal units while one gas unit is provided in Areas 2 and 3 respectively. Each control area is employed with WTG as additional generations. To get a realistic approach to the network, thermal generations are operational with suitable GRC and GDB of 3%/min and 0.06% respectively. The incremental power generation from WTG is fed to all control areas to maintain the power balance automatically. Also, the gas units are equipped with GRC of 20%/min. Six GENCOs and DISCOs are considered for investigation. Control Area 1 has two GENCOs and two DISCOs. Areas 2 and 3 have one GENCO and one DISCO each, and Area 4 has two GENCOs and two DISCOs. Aggregators in each control area collect EVs' information and fetch them to the control dispatch center. The capacity ratio of Area 1, 2, 3 and 4 are considered as 1:2:2:4.

2.1 Designing aspects of four area restructured system model

In a restructured environment, a DISCO participation matrix (DPM) provides information on the type of transaction i.e. the liberty of a GENCO in its area or other areas to agree with DISCOs in its area or other areas too [8, 32, 33]. Thirty-six contract participation factor elements in DPM exist with six GENCOs and DISCOs in total.

$$\mathrm{DPM} = \begin{bmatrix} \mathrm{cpf}_{11} & \mathrm{cpf}_{12} & \mathrm{cpf}_{13} & \mathrm{cpf}_{14} & \mathrm{cpf}_{15} & \mathrm{cpf}_{16} \\ \mathrm{cpf}_{21} & \mathrm{cpf}_{22} & \mathrm{cpf}_{23} & \mathrm{cpf}_{24} & \mathrm{cpf}_{25} & \mathrm{cpf}_{26} \\ \mathrm{cpf}_{31} & \mathrm{cpf}_{32} & \mathrm{cpf}_{33} & \mathrm{cpf}_{34} & \mathrm{cpf}_{35} & \mathrm{cpf}_{36} \\ \mathrm{cpf}_{41} & \mathrm{cpf}_{42} & \mathrm{cpf}_{43} & \mathrm{cpf}_{44} & \mathrm{cpf}_{45} & \mathrm{cpf}_{46} \\ \mathrm{cpf}_{51} & \mathrm{cpf}_{52} & \mathrm{cpf}_{53} & \mathrm{cpf}_{54} & \mathrm{cpf}_{55} & \mathrm{cpf}_{56} \\ \mathrm{cpf}_{61} & \mathrm{cpf}_{62} & \mathrm{cpf}_{63} & \mathrm{cpf}_{64} & \mathrm{cpf}_{65} & \mathrm{cpf}_{66} \end{bmatrix} \tag{1}$$

$$\begin{aligned} \Delta P_{\mathrm{tie13}} &= (\text{Power import from Area 3}) \\ &\quad - (\text{Power export to Area 1}) \\ &= (\mathrm{cpf}_{41} + \mathrm{cpf}_{42}) - (\mathrm{cpf}_{14} + \mathrm{cpf}_{24}). \end{aligned} \tag{2}$$

$$\begin{aligned} \Delta P_{\mathrm{tie23}} &= (\text{Power import from Area 3}) \\ &\quad - (\text{Power export to Area 2}) \\ &= (\mathrm{cpf}_{34} - \mathrm{cpf}_{43}). \end{aligned} \tag{3}$$

$$\begin{aligned} \Delta P_{\mathrm{tie34}} &= (\text{Power import from Area 4}) \\ &\quad - (\text{Power export to Area 3}) \\ &= (\mathrm{cpf}_{54} + \mathrm{cpf}_{64}) - (\mathrm{cpf}_{45} + \mathrm{cpf}_{46}). \end{aligned} \tag{4}$$

$$\begin{aligned} \Delta P_{\mathrm{tie34}} &= (\text{Power import from Area 4}) \\ &\quad - (\text{Power export to Area 3}) \\ &= (\mathrm{cpf}_{54} + \mathrm{cpf}_{64}) - (\mathrm{cpf}_{45} + \mathrm{cpf}_{46}). \end{aligned} \tag{5}$$

$$\begin{aligned} \Delta P_{\mathrm{tie24}} &= (\text{Power import from Area 4}) \\ &\quad - (\text{Power export to Area 2}) \\ &= (\mathrm{cpf}_{53} + \mathrm{cpf}_{63}) - (\mathrm{cpf}_{35} + \mathrm{cpf}_{36}). \end{aligned} \tag{6}$$

It can be observed from Fig. 1 that the exchanges of power among the control areas are given by Exch_1, Exch_2, Exch_3 and Exch_4 respectively. The tie-power flow exchanges among the control areas in terms of contracted power demand can be calculated as follows:

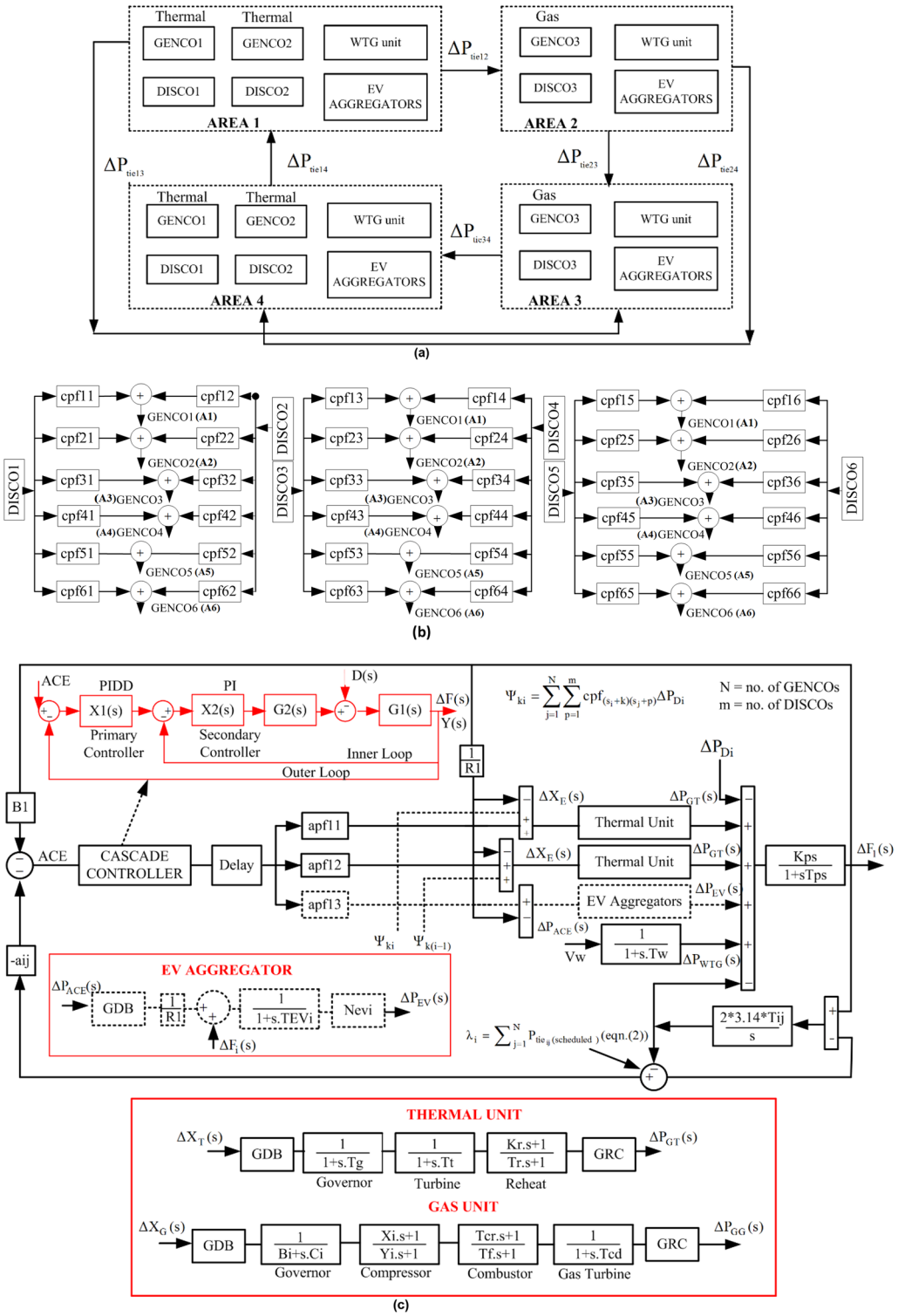

Fig.1 Schematic representation and system layout of the four- area hybrid system under restructured environment. **a** Schematic diagram of the four-area AGC model. **b** Description of DISCO participation matrix for the four-area AGC model in restructured environment. **c** Transfer function model and layout of Area 1 of the hybrid system under restructured environment (incorporating EV and WTG). **d** Transfer function model of the four area system under Restructured environment (without EV and WTG)

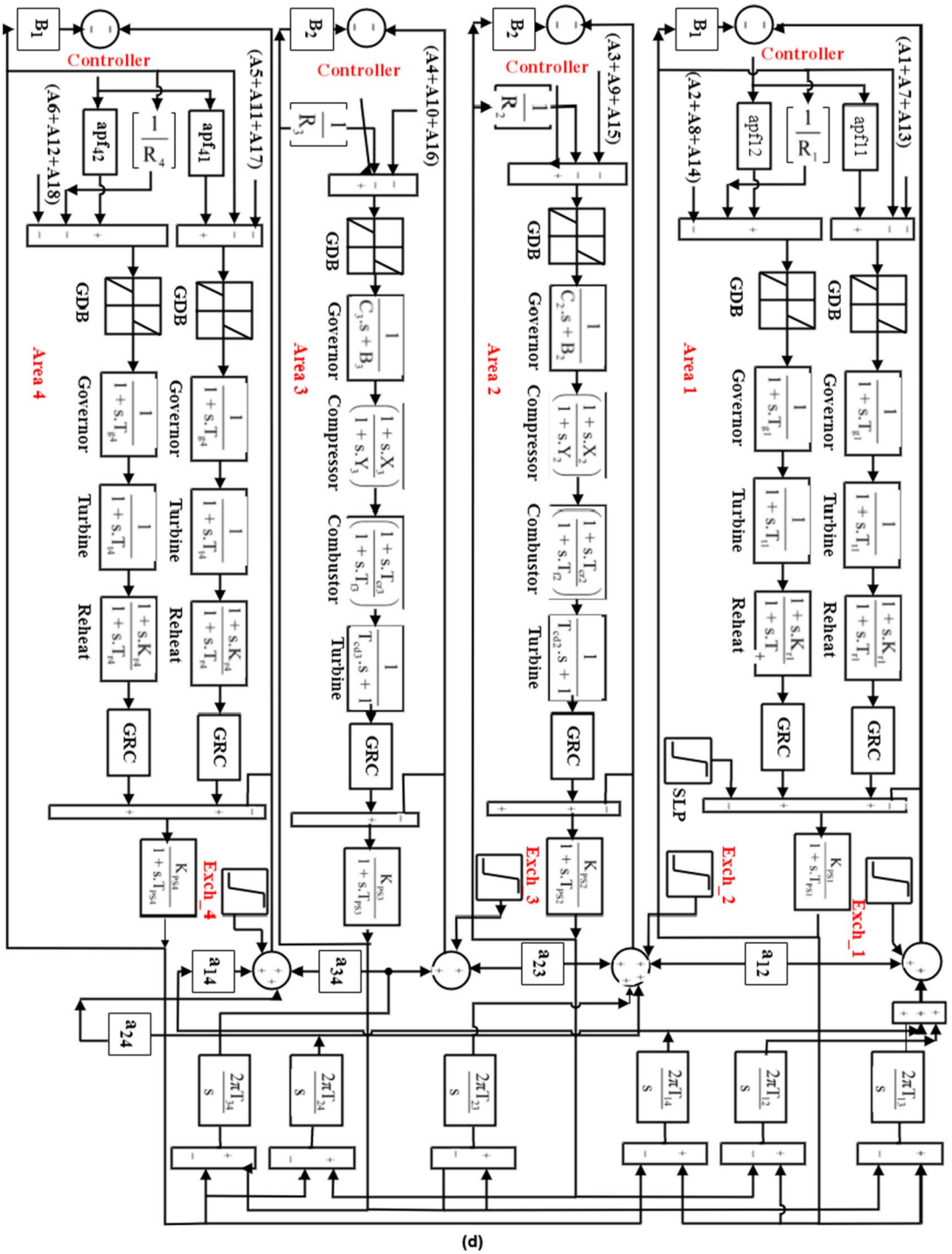

Fig.1 continued

$$\begin{aligned}\text{Exch\_1} = &[(\text{Demand in DISCOs in Area 2 from GENCOS in Area 1}) - (\text{Demand in DISCOs in Area 1 from GENCOS in Area 2})] \times \Delta P_{L1} \\ &+ [(\text{Demand in DISCOs in Area 3 from GENCOS in Area 1}) - (\text{Demand in DISCOs in Area 3 from GENCOS in Area 1})] \times \Delta P_{L1} \\ &+ [(\text{Demand in DISCOs in Area 4 from GENCOS in Area 1}) - (\text{Demand in DISCOs in Area 1 from GENCOS in Area 4})] \\ &\times \Delta P_{L1} = \Delta P_{tie12} + \Delta P_{tie13} + \Delta P_{tie14}. \end{aligned} \tag{7}$$

$$\begin{aligned}\text{Exch\_2} = &[(\text{Demand in DISCOs in Area 2 from GENCOS in Area 1}) \\ &- (\text{Demand in DISCOs in Area 1 from GENCOS in Area 2})] \\ &\times \Delta P_{L2} = \Delta P_{tie23}. \end{aligned} \tag{8}$$

$$\begin{aligned}\text{Exch\_3} = &[(\text{Demand in DISCOs in Area 2 from GENCOS in Area 1}) \\ &- (\text{Demand in DISCOs in Area 1 from GENCOS in Area 2})] \\ &\times \Delta P_{L3} = \Delta P_{tie34}. \end{aligned} \tag{9}$$

$$\begin{aligned}\text{Exch\_4} = &[(\text{Demand in DISCOs in Area 2 from GENCOS in Area 1}) \\ &- (\text{Demand in DISCOs in Area 1 from GENCOS in Area 2})] \\ &\times \Delta P_{L4} = \Delta P_{tie24}. \end{aligned} \tag{10}$$

The scheduled tie line power expression can be given as:

$\Delta P_{\text{tie, i–j (scheduled)}}$ = [Power supplied from GENCOs of ith area to DISCOs of jth area] – [Power supplied from GENCOs of jth area to DISCOs of ith area].

The tie-line error can be depicted by:

$$\Delta P_{\text{tie, i – j (error)}} = \Delta P_{\text{tie, i – j (actual)}} + \Delta P_{\text{tie, i – j (scheduled)}}. \tag{11}$$

2.2 Wind generator turbine

The electric power generation from WTG depends on wind velocity (V_W) which is comprised of base wind velocity (V_{WB}), wind gust velocity (V_{WG}), ramp wind velocity (V_R) and noise wind velocity (V_{WN}) as [21]:-

$$V_W = V_{WB} + V_{WG} + V_{WR} + V_N \tag{12}$$

The mechanical power output of WTG is given by:

$$P_w = \left(\frac{1}{2}\right)\rho C_p A_r v_\omega^3 \tag{13}$$

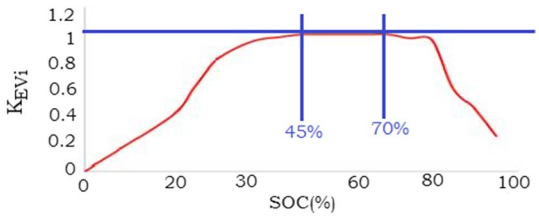

Fig. 2 Gain K_{EVi} versus state of charge (SOC)

where ρ (= 1.25 kg/m^3), C_p, A_r (= 1735 m^2) and v_w are the air-density, co-efficient of power, blade swept area and available wind speed respectively. It is a well known fact that the total system inertia decreases when there exists more intermittent source integration. The equivalent regulation constant increases thereby reducing the area frequency response characteristics [16]. Assuming R_W to be the amount of wind power participation in the grid [14], R_R is the amount of remaining conventional generation fed to the grid, and the modified inertia constant of the system can be expressed as:

$$H_{new,i} = H_{old,\,i}[1 + (R_W - R_R)] \tag{14}$$

The modified equivalent speed regulation constant is:

$$R_{new,i} = \frac{R_{old,i}}{[1 + (R_W - R_R)]} \tag{15}$$

The modified AFRC is expressed as follows:

$$\beta_{new,i} = B_{new,i} = \frac{1}{R_{old,i}}[1 + (R_W - R_R)] + D_i \tag{16}$$

Changes in R_i and β_i result in a new area control error given by:

$$ACE_{new,i} = \Delta P_{tie,i} + \beta_{new,i}\Delta F_i.$$

2.3 EV aggregators

EV batteries connected to the power system with battery chargers regulating the power between the DC and AC are constituent of EV aggregators. A dead band function along with droop control R is present with upper and lower bounds as primary governor control. R depends on the charge of the system (known as the state of charge) and is introduced in the system with a participation factor [34]. During the peak hours, EV gets charged from the grid while EV gets discharged during off-peak hours [23, 24]. The range of charge–discharge for the EV is considered as ± 5 kW but it is allowed to charge to 50 kW or even more with rapid charging. EV participates to reduce the area control error for secondary control of frequency.

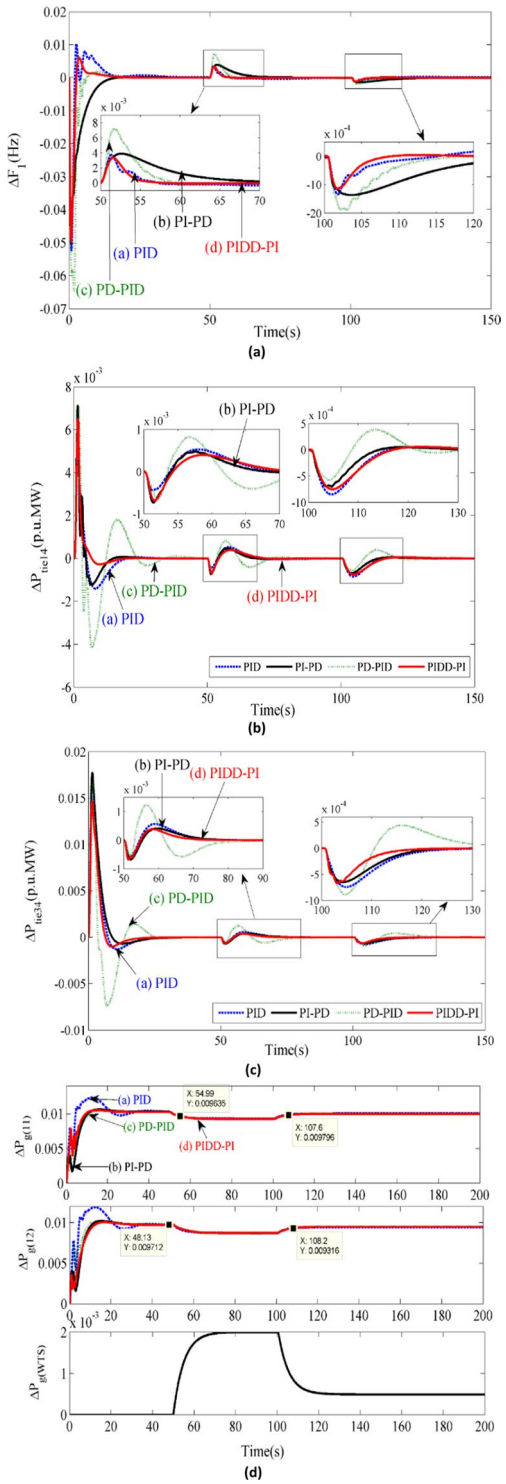

Fig. 3 Comparison of performance of PID, PI-PD, PD-PID and PIDD-PI during bilateral transactions. **a** Frequency deviation in Area 1. **b** Tie-power deviation in the line connecting Area 1 and 4. **c** Tie-power deviation in the line connecting Area 3 and 4. **d** Power generation in thermal plant and WTG unit in Area 1

The SOC needs to be more than 20% if the PEV battery in charging mode is introduced to primary control (Fig. 2). For SOC below 45% or above 70%, K_{EVi} lies between $0 < K_{EVi} < 1$ and $K_{EVi} = 1$ between 45 and 70%. The highest and lowest amount of EV fleets' power capacity is given by ΔP_{AG}^{max} and ΔP_{AG}^{min} as:

$$\Delta P_{AG}^{max} = +\left[\frac{1}{N_{EVi}} \times \Delta P_{EVi}\right] \tag{17}$$

$$\Delta P_{AG}^{min} = -\left[\frac{1}{N_{EVi}} \times \Delta P_{EVi}\right]. \tag{18}$$

2.4 Design and tuning of PIDD-PI controller

The basis behind cascade controller configuration (Fig. 1c) is that the model controlled inner loop overcomes the integral anti-windup that may saturate the inner control loop. This may result in a track mismatch of the outer loop with inner loop controllers as the output of G2 is directly fed into G1. The main functions of cascade control are: (a) in presence of external or internal disturbance, whether the inner control has any effect on the outer control and (b) outer process to ensure the output process quality. The external loop equation relating the process output Y(s), outer process, and load disturbance D(s) is given as [27, 28].

$$Y_1(s) = G_1(s) \times X_1(s) + D(s) \tag{19}$$

The inner control is given as:

$$Y_2(s) = G_2(s) \times X_2(s) \tag{20}$$

In this paper, PIDD forms the constituent of single-loop control followed by a PI controller in cascade (Fig. 1c). Reference track and disturbance rejection are carried out with the responses. Two controllers X1(s) and X2(s) are named as the outer and the inner controllers respectively. There are chances of further disturbances due to the additional derivative parameter caused by continuous fluctuation in load demand. Thus a filter is added to minimize the undesirable effect of high-frequency noise. Here, the PI controller is made as the inner and PIDD as the outer controllers.

$$X_1(s) = K_P + \frac{K_I}{s} + \frac{Ns^2}{(N+s)}K_D \tag{21}$$

$$X_2(s) = K_{PP} + \frac{K_{II}}{s} \tag{22}$$

Table 1 Optimum parameters for PID, PD-PID, PI-PD and PIDD-PI controller under bilateral transactions

Controller gains	PID	PD-PID	PI-PD	PIDD-PI
Area 1 (outer loop)				
K_{P1}*	0.7623	0.6428	0.2526	0.8654
K_{I1}*	0.8317	–	0.7773	0.1727
K_{DD1}*	0.6369	0.5850	–	0.4620
N_1*	34.141	–	–	27.036
Area 2 (outer loop)				
K_{P2}*	0.4871	0.6232	0.5930	0.6698
K_{I2}*	0.6783	–	0.9759	0.2318
K_{DD2}*	0.5669	0.4161	–	0.1919
N_2*	75.944	–	–	54.385
Area 3 (outer loop)				
K_{P3}*	0.6656	0.8079	0.7394	0.6161
K_{I3}*	0.8552	–	0.7035	0.3981
K_{DD3}*	0.5600	0.4773	–	0.2848
N_3*	60.358	–	–	10.075
Area 4 (outer loop)				
K_{P4}*	0.1966	0.7248	0.5771	0.8909
K_{I4}*	0.9992	–	0.9986	0.2990
K_{DD4}*	0.2077	0.6629	–	0.8387
N_4*	69.177	–	–	39.685
Area 1 (inner loop)				
K_{PP1}*	–	0.6779	0.7904	0.9638
K_{IP1}*	–	0.9358	–	0.9330
K_{D1}*	–	0.4908	0.3783	–
N_{C5}*	–	41.764	87.572	–
Area 2 (inner loop)				
K_{PP2}*	–	0.5718	0.4939	0.9776
K_{II2}*	–	0.6510	–	0.2645
K_{D2}*	–	0.6627	0.4525	–
N_{C2}*	–	42.756	41.856	–
Area 3 (inner loop)				
K_{PP3}*	–	0.5201	0.7459	0.9140
K_{II3}*	–	0.7932	–	0.1336
K_{D3}*	–	0.3259	0.5719	–
N_{C3}*	–	76.152	57.746	–
Area 4 (inner loop)				
K_{PP4}*	–	0.3118	0.9363	0.3332
K_{IP4}*	–	0.9998	–	0.9837
K_{D4}*	–	0.2759	0.2216	–
N_{C4}*	–	38.186	44.396	–

* represents optimum values for the PIDD - PI controller using Harris Hawk Algorithm

$$Y(s) = \left[\frac{G_1(s)G_2(s)C_1(s)}{1 + G_2(s)C_2(s) + G_1(s)G_2(s)C_1(s)C_2(s)}\right]R(s) - \left[\frac{G_1(s)}{1 + G_2(s)C_2(s) + G_1(s)G_2(s)C_1(s)C_2(s)}\right]D(s) \quad (23)$$

$G_1(s)$ and $G_2(s)$ are the primary and secondary control loops respectively, while D(s) is the load disturbance. For simultaneous tuning of controller parameters of PIDD-PI controller, a recently introduced algorithm named "Harris Hawks Optimization" (HHO) is used. The formulation of the above constrained optimization problem is as follows:

Table 2 Comparison of Performance improvement of PIDD-PI over PID, PI-PD and PD-PID controllers

Response	Controllers				% Improvement of PIDD-PI over		
	PID	PI-PD	PD-PID	PIDD-PI	PID	PI-PD	PD-PID
ΔF_1 Figure 3a							
POS	0.0230	–	–	0.0060	73.91	NA	NA
PUS	0.0600	0.0620	0.0670	**0.0500**	16.67	19.35	25.37
ST	34.160	24.190	35.160	**11.060**	67.62	53.86	68.44
ΔP_{tie14} Figure 3b							
POS	0.0056	0.0070	0.0070	0.0060	NA	14.28	14.28
PUS	0.0024	0.0013	0.0039	**0.0002**	91.67	64.61	94.87
ST	36.000	16.150	36.080	**15.250**	57.63	5.9	57.73
ΔP_{tie34} Figure 3c							
POS	0.0154	0.0170	0.0070	0.0140	90.09	17.64	50
PUS	0.0014	0.0010	0.0170	**0.0010**	28.57	Equal	94.11
ST	25.140	26.840	33.930	**20.100**	25.07	25.11	68.80

Bold representes the best values obtained with PIDD - PI controller when compared with the other comtrollers tabulated such as PID, PI-PD, PD-PID

$$J_{ITAE} = \int_0^t \left\{(\Delta F_i) + \left(\Delta P_{tie\,i\,-\,j}\right)\right\}.tdt \tag{24}$$

Minimize the objective function J_{ACE} such that:

$$K_{Pi}^{min} \le K_{Pi} \le K_{Pi}^{max}; \quad K_{PPi}^{min} \le K_{PPi} \le K_{PPi}^{max}$$

$$K_{Ii}^{min} \le K_{Ii} \le K_{Ii}^{max}; \quad K_{IIi}^{min} \le K_{IIi} \le K_{IIi}^{max}$$

$$K_{Di}^{min} \le K_{Di} \le K_{Di}^{max}; \quad N_i^{min} \le N_i \le N_i^{max}$$

where K_{Pi}^{max}, K_{Pi}^{min}, K_{Ii}^{max}, K_{Ii}^{min}, K_{PPi}^{max}, K_{PPi}^{min}, K_{IIi}^{max}, K_{IIi}^{min}, N_i^{max}, and N_i^{min} represent the maximum and minimum values of controller parameters, respectively. The HHO algorithm is employed to evaluate the optimum controller gains and other parameters of the proposed cascade controller in which the candidates/populations are the Harris Hawks and the optimal global solution is the intended prey that tends to escape from time to time. The HHO technique's tuned parameters are taken with 50 search agents, and maximum number of iteration of 50. The tuned parameters are fixed by minimising the cost function over 40 trials.

3 Results and analysis

The proposed hybrid system is executed for the bilateral transaction, contract violation, outage of a generating unit and thereby decline in inertia, and robustness analysis with: (1) higher load demand (2) communication delays; (3) system loading and (4) change in time constants of the gas generating unit.

3.1 Bilateral transactions

First, a DPM is chosen to explain the case of bilateral transactions, where any GENCOs of any area can contract with any DISCOs in any area. Active power of 0.01 p.u is contracted between each DISCO and GENCO. Considering the above DPM, GENCOs in Area 1, 2, 3 and 4 should generate active power of 0.02 p.u., 0.01 p.u., 0.01 p.u. and 0.02 p.u. respectively.

$$DPM_A = \begin{bmatrix} 0.2 & 0.1 & 0.2 & 0.2 & 0.2 & 0.1 \\ 0.2 & 0.2 & 0.1 & 0.1 & 0.2 & 0.2 \\ 0.1 & 0.2 & 0.1 & 0.2 & 0.2 & 0.2 \\ 0.2 & 0.1 & 0.2 & 0.1 & 0.2 & 0.2 \\ 0.1 & 0.2 & 0.2 & 0.2 & 0.1 & 0.2 \\ 0.2 & 0.2 & 0.2 & 0.2 & 0.1 & 0.1 \end{bmatrix} \tag{25}$$

Again, WTG is employed in each control area, and provide active power output of 0.002 p.u. from 50–100 s and 0.0005 p.u.from 100–200 s to the grid as shown in Fig. 3d.

Thus, the remaining power after considering power output from WTG, i.e. (0.02–0.002 = 0.018 p.u), (0.01–0.002 = 0.008 p.u.), (0.01–0.002 = 0.008 p.u.) and (0.02–0.002 = 0.018 p.u) accordingly should be generated by the GENCOs in each area, respectively. Using DPM, $\Delta P_{tie1\text{-}2} = (0.2 + 0.1) - (0.1 + 0.2) = 0$ p.u. Similarly, the schedule tie line power between Area 1 and 2 is: $\Delta P_{tie1\text{-}2} = \Delta P_{tie1\text{-}2} = \Delta P_{tie1\text{-}2} = \Delta P_{tie1\text{-}2} = \Delta P_{tie1\text{-}2} = 0$ p.u.

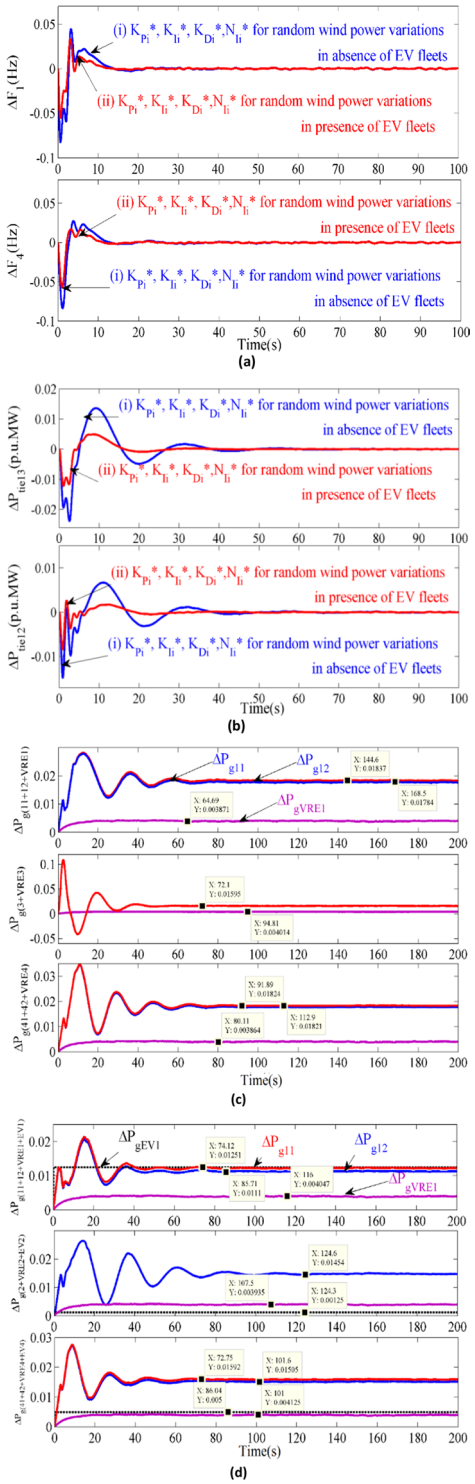

Fig. 4 Comparison of system dynamic responses during contract violation to show the effect of EV aggregators. **a** Frequency deviation (Area 1 and 4). **b** Tie-power deviation (in the line connecting area 1 and 3; area 1 and 2). **c** Power generation in absence of EV aggregators (Area 1, 3 and 4). **d** Power generation in presence of EV aggregators (area 1, 2 and 4)

The system is equipped with a non-cascade controller such as PID and a cascade controller such as PI-PD, PD-PID and PIDD-PI. These controllers are used as secondary controllers and parameters are optimized using the HHO technique. The optimized parameters for the aforesaid controllers are shown in Table 1.The cost function J_{ITAE} for PID, PI-PD, PD-PID and PIDD-PI controllers are noted as 0.0718, 0.0674, 0.0370 and 0.0214, respectively. The system dynamic responses corresponding to optimum parameters of each controller are obtained and are shown in Fig. 3.

From the J_{ITAE} values and Fig. 3, the dominance of PIDD-PI over PID, PI-PD and PD-PID controller can be easily inferred for the proposed hybrid system. Figure 3d shows the change in $\Delta P_{g(WTS)}$ due to the change in V_w. Furthermore, the system responses of electricity generations from thermal (ΔP_{g11}, ΔP_{g12}, ΔP_{g41}, ΔP_{g42}) and gas generators (ΔPg_2, ΔPg_3) of the respective areas are evident of being regulated (only power generation in Area 1 is shown). The significant improvement of PIDD-PI controller over PID, PI-PD and PD-PID are tabulated in Table 2 and Fig. 3a–c. The settling time and peak undershoot in case of PIDD—PI controller is seen to outperform others, whereas the peak overshoot is either equal or similar with the others. Thus, it can be inferred that PIDD—PI controller is superior in terms of less time to settle and lower maximum undershoot with almost similar peak overshoot against PID and other cascade controllers.

3.2 Contract violation (nominal case)

Here, DISCOs in all areas demand more power, violating the contracts and needing to be compensated by individual generators. The compensation of uncontracted load is encouraged through EV aggregators because of rapid starting characteristics of EVs. 250 discharged EVs are considered in Area 1, while 600 EVs are considered in each of the other areas. Assuming each DISCO requires excess load of 0.01 p.u. so some loads in Area 1, 2, 3 and 4 becomes 0.04 p.u., 0.02 p.u. 0.02 p.u. and 0.04 p.u. respectively. The total number of 2050 EVs will share a certain percentage of the unscheduled power by discharging. As an incremental power output of WT is provided in each area, a portion of load demand will be maintained at the same level. The PIDD—PI cascade controller is employed as secondary controller for the evaluation and the HHO technique is employed to tune the gains and other parameters of the controller. The corresponding system responses are plotted, compared and presented in Fig. 4a–d.

Based on market information, area participation factors (apf's) are considered such that the thermal units

Table 3 Optimum parameters of PIDD-PI controller during contract violation of 2% from nominal 2%

	K_{P1}*	K_{I1}*	K_{DD1}*	N_1*	K_{P2}*	K_{I2}*
wEV	0.940	0.260	0.307	32.66	0.800	0.447
woEV	0.765	0.323	0.427	40.07	0.666	0.497
	K_{DD2}*	N_2*	K_{P3}*	K_{I3}*	K_{DD3}*	N_3*
wEV	0.562	52.83	0.888	0.283	0.283	36.02
woEV	0.623	59.14	0.739	0.452	0.290	37.38
	K_{P4}*	K_{I4}*	K_{DD4}*	N_4*	K_{PP1}*	K_{II1}*
wEV	0.535	0.612	0.452	48.19	0.544	0.617
woEV	0.349	44.32	0.538	0.552	0.523	0.534
	K_{PP2}*	K_{II2}*	K_{PP3}*	K_{II3}*	K_{PP4}*	K_{II4}*
wEV	0.490	0.550	0.460	0.245	0.740	0.584
woEV	0.523	0.534	0.409	0.267	0.652	0.427

* represents optimum values for the PIDD - PI controller using Harris Hawk Algorithm

Table 4 Modified R, B, T_{PS} when inertia is reduced by 0%, 10%, 20%, 30%, 40%, 50% and 60% in area 1

	Reduction of inertia by						
	0%	10%	20%	30%	40%	50%	60%
H	5.00	4.50	4.00	3.50	3.00	2.50	2.00
T_{PS}	20.0	18.0	16.0	14.0	12.0	10.0	8.00
R	2.40	2.67	3.00	3.42	4.00	4.80	6.00
B	0.42	0.46	0.34	0.30	0.25	0.21	0.17

in Area 1 share 0.012 p.u and 0.011 p.u. power respectively, while EV aggregators discharges 0.012 p.u. power. Thus, (0.012 + 0.011 + 0.012 = 0.036 p.u.) along with 0.004 p.u. from WT confirm the generation of 0.04 p.u. within which the uncontracted load of 0.02 p.u. has been shared. To understand the effect of EV aggregators, the same is optimized in presence and in absence of EV aggregators, and are tabulated in Table 3.

Similarly, gas units and EV aggregators in area 2 and 3 contributes and discharge 0.0145 p.u. and 0.0012 p.u. power (total $\text{power}_{area2} = 0.0145 + 0.0012 + 0.004 = 0.02$ p.u.) 012 p.u. and 0.004 p.u. (total $\text{power}_{area3} = 0.012 + 0.004 + 0.004 = 0.02$ p.u.MW) respectively. The thermal units and EV aggregators in area 4 contributes (0.0159 + 0.0150 = 0.030 p.u.MW) and 0.005 p.u.MW power, respectively (total $\text{power}_{area4} = 0.030 + 0.005 + 0.004 = 0.04$ p.u.MW). The apf are taken as $apf_{11} = 0.34$, $apf_{12} = 0.34$, $apf_{13} = 0.32$; $apf_{21} = 0.92$, $apf_{22} = 0.08$; $apf_{31} = 0.75$, $apf_{32} = 0.25$; $apf_{41} = 0.44$, $apf_{42} = 0.41$, $apf_{43} = 0.138$. The generation schedule without EV aggregators is presented in Fig. 4d. This matches the generation profile.

3.3 Sudden outage of a thermal unit in area 1

Assume a contingency occurs in the system and there is an outage of a thermal unit in area 1 which results in reduction of inertia as well as capacity of area1. Because of the presence of a WTG unit, an analysis is carried out with inertia reduction of area 1 by 0–60% in steps of 20%. The modified R, B and T_{PS} are shown in Table 4. The system considered here for investigation is similar to the previous one in Sect. 3.2 apart from the fact that in Area 1, the values of H, R, B and T_{PS} are modified as in Table 4. The PIDD-PI controller is used as a secondary regulator in all control areas and the HHO optimized controller parameters are tabulated in Table 5. Figure 5 shows the responses when the inertia is reduced because of the penetration of renewable sources.

From Fig. 5, it can be inferred that the governor response becomes less sensitive beause of the decrement in inertia and aptitude to control the power output of the grid connected system. It results in further frequency deviation and a long settling time. Also, the tie-power deviation experiences more oscillations when the inertia declines gradually.

Table 5 Optimum controller gains with contract violation of 2% and reduced inertia of 20%, 40% and 60%

Controller gains	20% reduction		40% reduction		60% reduction	
	wEV	WoEV	Wev	woEV	wEV	woEV
Area 1 (outer loop)						
K_{P1}*	0.866	0.853	0.882	0.933	0.932	0.889
K_{I1}*	0.504	0.002	0.129	0.002	0.191	0.001
K_{DD1}*	0.220	0.485	0.501	0.470	0.658	0.551
N_1*	20.14	41.30	35.81	31.29	43.89	26.87
Area 2 (outer loop)						
K_{P2}*	0.603	0.626	0.675	0.547	0.655	0.677
K_{I2}*	0.594	0.447	0.623	0.626	0.611	0.653
K_{DD2}*	0.524	0.582	0.648	0.625	0.592	0.666
N_2*	47.82	72.01	61.69	59.09	66.80	60.65
Area 3 (outer loop)						
K_{P3}*	0.890	0.858	0.731	0.772	0.700	0.724
K_{I3}*	0.390	0.465	0.533	0.575	0.570	0.679
K_{DD3}*	0.282	0.284	0.246	0.310	0.279	0.396
N_3*	34.01	23.86	37.96	26.26	34.05	22.94
Area 4 (outer loop)						
K_{P4}*	0.560	0.458	0.383	0.499	0.369	0.504
K_{I4}*	0.574	0.604	0.662	0.640	0.757	0.665
K_{DD4}*	0.312	0.380	0.256	0.483	0.390	0.426
N_4*	69.08	48.11	54.04	61.24	39.03	67.96
Area 1 (inner)						
K_{PP1}*`	0.749	0.306	0.614	0.449	0.754	0.412
K_{II1}*	0.582	0.561	0.541	0.515	0.503	0.528
Area 2 (inner)						
K_{PP2}*	0.628	0.442	0.582	0.464	0.658	0.440
K_{II2}*	0.570	0.498	0.707	0.482	0.570	0.552
Area 3 (inner)						
K_{PP3}*	0.414	0.371	0.530	0.461	0.488	0.418
K_{II3}*	0.395	0.347	0.210	0.239	0.095	0.211
Area 4(inner)						
K_{PP4}*	0.739	0.680	0.789	0.637	0.710	0.648
K_{II4}*	0.614	0.368	0.647	0.395	0.656	0.537

3.4 Examining the proposed PIDD-PI cascade controller's robustness

As stated in the literature, participation of EV aggregators in a smart grid requires open communication channels which may be stochastic in nature. Also, load demand in a control area may not follow the contracted demand and may violate in urging more power from any GENCO. Therefore, it is of utmost interest to ensure the toughness of the projected cascade controller. Thus, four scenarios are considered here for investigation namely (1) increase in load demand from nominal 4% (Sect. 3.2) to 8% and 10% (2) open communication channels of 50 ms, 100 ms and 300 ms time delay; (3) ± 25% change in system loading and (4) ± 25% change in gas generating unit parameters (C_i, T_f and T_{cd}) simultaneously.

The HHO method is again used to optimize the regulator parameters at changed conditions which are tabulated in Tables 6 and 7. The dynamic responses at changed condition are compared with dynamic responses obtained at nominal condition (Sect. 3.2) and are depicted in Fig. 6. Specifically, Fig. 6a depicts the frequency deviation in area 1 at higher violations

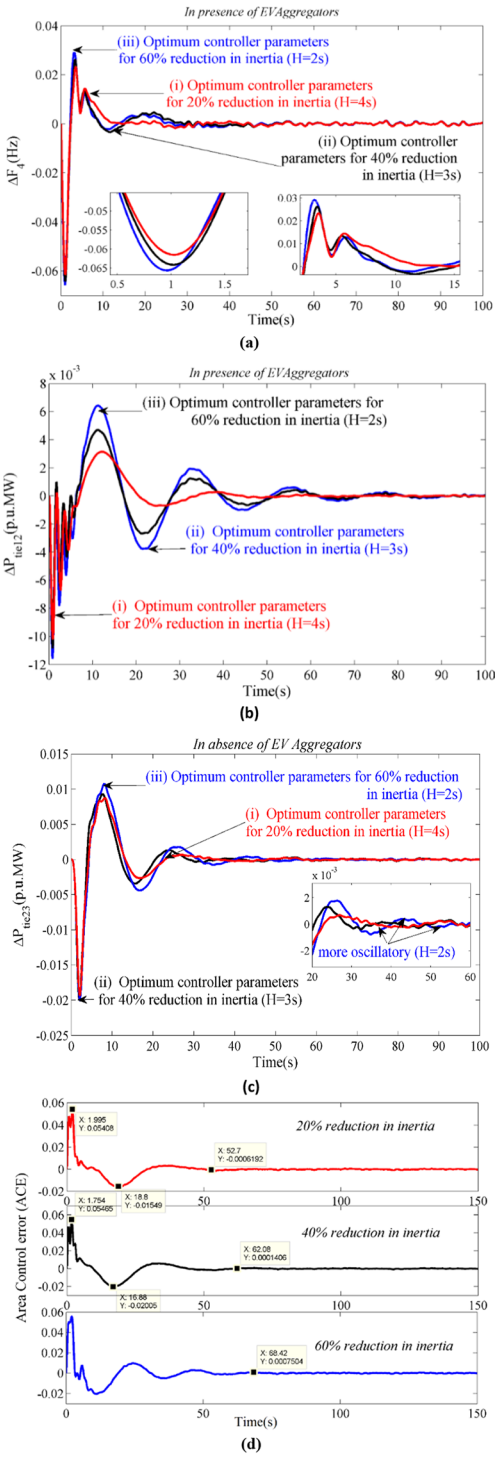

Fig. 5 Comparison of system dynamic responses due to outage of a thermal unit considering the effect of R, B. **a** Frequency deviation in area 4 in presence of EV aggregators. **b** Tie-power deviation in the line connecting area 1 and 2 in presence of EV Aggregators. **c** Tie-power deviation in the line connecting area 2 and 3 in absence of EV Aggregators. **d** Control signal in area 1 for 20%, 40% and 60% reduction in inertia respectively in presence of EV Aggregators

of contract and both responses exhibit almost similar routine in terms of time to settle. But as the load demand increases, both the peak overshoot and peak undershoot increase. The uncontracted demands of 4% (4 + 4 = 8%) and 6% (4 + 6 = 10%) have been attained by the conventional generations, WTG unit and EV aggregators as shown in Fig. 6b. Moreover, the proposed controller responds well to open communication channels of $\tau(t) = 50$ ms and 100 ms. However, the same becomes unstable when controller gains are optimized at $\tau(t) = 300$ ms (Fig. 6d). Generation profile of 6% extra demand from Area 1 is easily mitigated by the local GENCOs as confirmed from Fig. 6b.

Figure 7 represents the system dynamics without consideration of additional energy from WTG. Specifically, Fig. 7a, b depict the frequency change and tie-power change for ± 25% change in system loading. Also, Fig. 7c, d depict the system responses when there is a ± 25% change in gas generating unit parameters (C_i, T_f and T_{cd}). The responses reveal that both changed conditions offer similar performance except peak deviations are slightly different but are within a satisfactory limit. The EV aggregators in conjunction with the proposed controller gains have shown satisfactory performance, with the robust controller settings not required to reset during change in higher contract violations, time delay of 50 ms and 100 ms, and system loading and time constants of the gas generating unit.

3.5 Convergence characteristics of different algorithms

It is observed that the Harris hawk algorithm has successfully optimized twenty-four parameters simultaneously in a system. In this case study, HHO is compared with other powerful algorithms such as the Quasi Oppositional Harmony Search Algorithm (QOHSA) [7, 8], Biogeography Based Optimization (BBO) [13] and the Bat Algorithm (BA) [28]. These algorithms have been successfully applied in optimizing different parameters under AGC studies in both a conventional and deregulated environment. For effective comparison, the population size and maximum generation for each algorithm are both kept the same at 50. One of the previous case studies in Sect. 3.4 where the load demand is increased from 4 to 8% is considered here for investigation and each algorithm is employed one by one to plot the convergence characteristics. The responses are compared and are shown in Fig. 8 which clearly establishes that the HHO algorithm converges at a lower J_{ITAE} value than the other algorithms but the time of convergence is almost the same for all (100 s). Thus, HHO outperforms others in terms of lower J_{ITAE} values.

Table 6 Optimum regulator parameters during higher SLP of 6% and 10% and communication delays of $\tau(t)=50$ ms,100 ms and 300 ms

Controller gains	SLP = 6%	SLP = 10%	τ = 50 ms	τ = 100 ms	τ = 300 ms
Area 1 (outer loop)					
K_{P1}*	0.8452	0.7872	0.9830	0.8441	0.8119
K_{I1}*	0.0017	0.0017	0.1213	0.3207	0.3930
K_{DD1}*	0.3336	0.4254	0.5738	0.3280	0.4732
N_1*	36.992	36.599	37.238	46.425	38.192
Area 2 (outer loop)					
K_{P2}*	0.7319	0.6660	0.7410	0.7344	0.2809
K_{I2}*	0.3551	0.5742	0.6566	0.3935	0.6627
K_{DD2}*	0.7061	0.7164	0.8252	0.5692	0.3092
N_2*	84.231	74.512	59.928	64.992	64.008
Area 3 (outer loop)					
K_{P3}*	0.8638	0.6529	0.8250	0.8393	0.5074
K_{I3}*	0.4244	0.5057	0.6788	0.3654	0.5130
K_{DD3}*	0.3628	0.4420	0.4615	0.3021	0.4159
N_3*	24.947	25.698	24.678	39.848	39.865
Area 4 (outer loop)					
K_{P4}*	0.5351	0.4315	0.7050	0.5928	0.4789
K_{I4}*	0.5351	0.6878	0.8943	0.8216	0.4489
K_{DD4}*	0.5351	0.4284	0.4855	0.4489	0.5320
N_4*	48.197	55.696	58.974	48.131	72.664
Area 1 (inner)					
K_{PP1}*	0.4356	0.4209	0.3920	0.5617	0.4536
K_{II1}*	0.5340	0.5432	0.6711	0.5418	0.4410
Area 2 (inner)					
K_{PP2}*	0.3746	0.5558	0.4272	0.4344	0.5063
K_{II2}*	0.4224	0.5496	0.2887	0.5086	0.1108
Area 3 (inner)					
K_{PP3}*	0.3347	0.3291	0.3263	0.3245	0.2439
K_{II3}*	0.1835	0.0889	0.1026	0.1325	0.0712
Area 4 (inner)					
K_{PP4}*	0.7406	0.6643	0.6773	0.6060	0.5120
K_{II4}*	0.5841	0.4491	0.7002	0.6278	0.5559

* represents optimum values for the PIDD - PI controller using Harris Hawk Algorithm

4 Conclusion

This paper investigates a cascade controller-based AGC of a four area hybrid power system with six GENCOs, six DISCOs and integrated wind power generation in a restructured environment. The system is investigated for bilateral transactions and contract violation scenarios. The following are the outcomes:

PIDD-PI as secondary controller outperforms PID, PI-PD and PD-PID in terms of fast settling time and peak undershoot. The peak overshoot remains similar to other controllers.

(a) EV aggregators mitigate the uncontracted demand of 1% from every DISCO in each area (4% in Area 1, 2% in Area 2, 2% in Area 2 and 4% in Area 4) along with conventional units, and assist in reducing frequency and tie-power deviation.

(b) Sudden outage of a thermal unit in Area 1 leads to decrease in the sum of total system inertia (Area 1 has only one thermal unit and WTG unit) and AFRC because the regulation constant is increased. With a decline of inertia, system oscillation increases, resulting in higher overshoot and undershoot along with prolonged time to settle down the ACE.

(c) Further robustness of the PIDD-PI controller is exhibited against realistic non-linearity such as 4% and 6% violation of contracts, stochastic communi-

Table 7 Optimum controller gains and parameters for ± 25% change in system loading, ± 25% change in C_i, T_f and T_{cd} of gas generating unit

Controller gains	Change in loading		Change in C_i, T_f, T_{cd}	
	+ 25%	-25%	+ 25%	-25%
Area 1 (outer loop)				
K_{P1}*	0.7663	0.8307	0.8307	0.8307
K_{I1}*	0.6251	0.3890	0.3890	0.3890
K_{DD1}*	0.7534	0.6608	0.6608	0.6608
N_1*	22.712	38.553	38.553	38.553
Area 2 (outer loop)				
K_{P2}*	0.7773	0.7527	0.7527	0.7527
K_{I2}*	0.4638	0.4785	0.4785	0.4785
K_{DD2}*	0.4717	0.7170	0.7170	0.7170
N_2*	63.520	66.123	66.123	66.123
Area 3 (outer loop)				
K_{P3}*	0.6973	0.3814	0.9062	0.9062
K_{I3}*	0.7261	0.0417	0.5675	0.5675
K_{DD3}*	0.2006	0.3066	0.3066	0.3066
N_3*	22.772	28.198	28.198	28.198
Area 4 (outer loop)				
K_{P4}*	0.7137	0.6058	0.6058	0.6058
K_{I4}*	0.5524	0.6665	0.6665	0.6665
K_{DD4}*	0.5118	0.4177	0.4177	0.4177
N_4*	67.206	65.323	65.323	65.323
Area 1 (inner)				
K_{PP1}*	0.5943	0.3060	0.3060	0.3060
K_{II1}*	0.6099	0.7001	0.7001	0.7001
Area 2 (inner)				
K_{PP2}*	0.7336	0.4105	0.4105	0.4105
K_{II2}*	0.2560	0.1446	0.1446	0.1446
Area 3 (inner)				
K_{PP3}*	0.5301	0.3814	0.3814	0.3814
K_{II3}*	0.1369	0.0417	0.0417	0.0417
Area 4 (inner)				
K_{PP4}*	0.5956	0.6718	0.6718	0.6718
K_{II4}*	0.8499	0.9417	0.9417	0.9417

* represents optimum values for the PIDD - PI controller using Harris Hawk Algorithm

cation delays of 50 ms, 100 ms and 300 ms, ± 25% of system loading and ± 25% of variation time constants C_i, T_f and T_{cd}.

(d) It is recommended to employ more EV aggregators to make the system operate in a stable condition at $\tau(t) = 300$ ms. Thus, in the presence of EV aggregators, the nominal controller parameters obtained at contract violation (Sect. 3.2) are not required to reset except for $\tau(t) = 300$ ms.

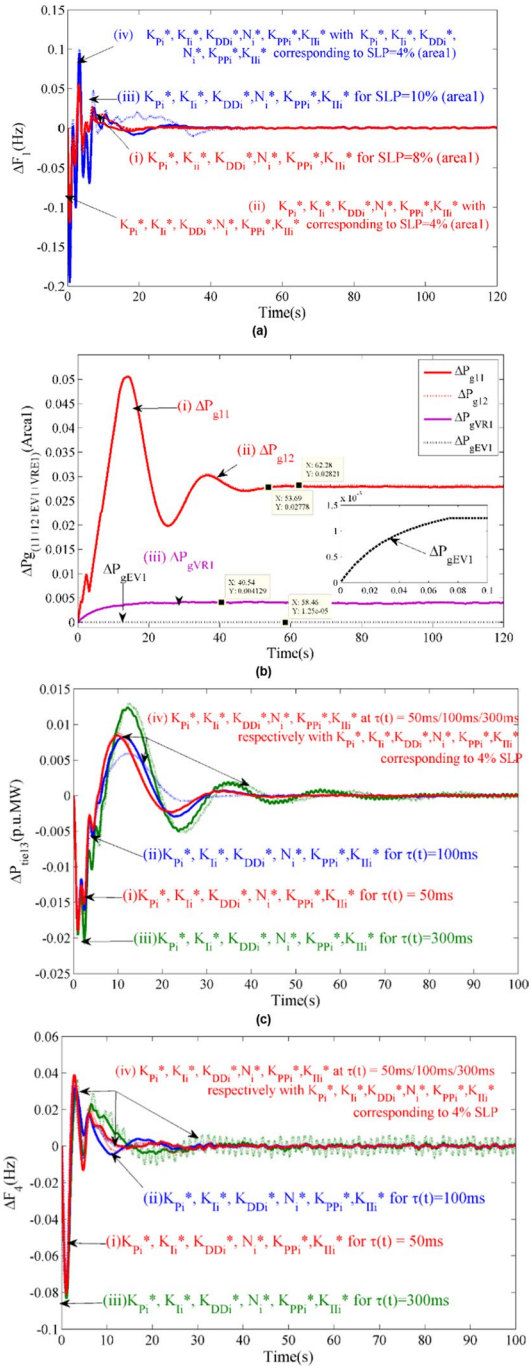

Fig. 6 Comparison of system dynamic responses during higher violation of contracted demand and different time delays in the system. **a** Frequency deviation in area 1 for 4% and 6% violations in contracted demand from nominal one. **b** Power generation in area 1 for 6% violations in contracted demand from nominal one. **c** Tie-power deviation in line connecting Area 1 and 3 for open communication channels of 50, 100 and 300 ms. **d** Frequency deviation in area 4 for open communication channel delays of 50, 100 and 300 ms

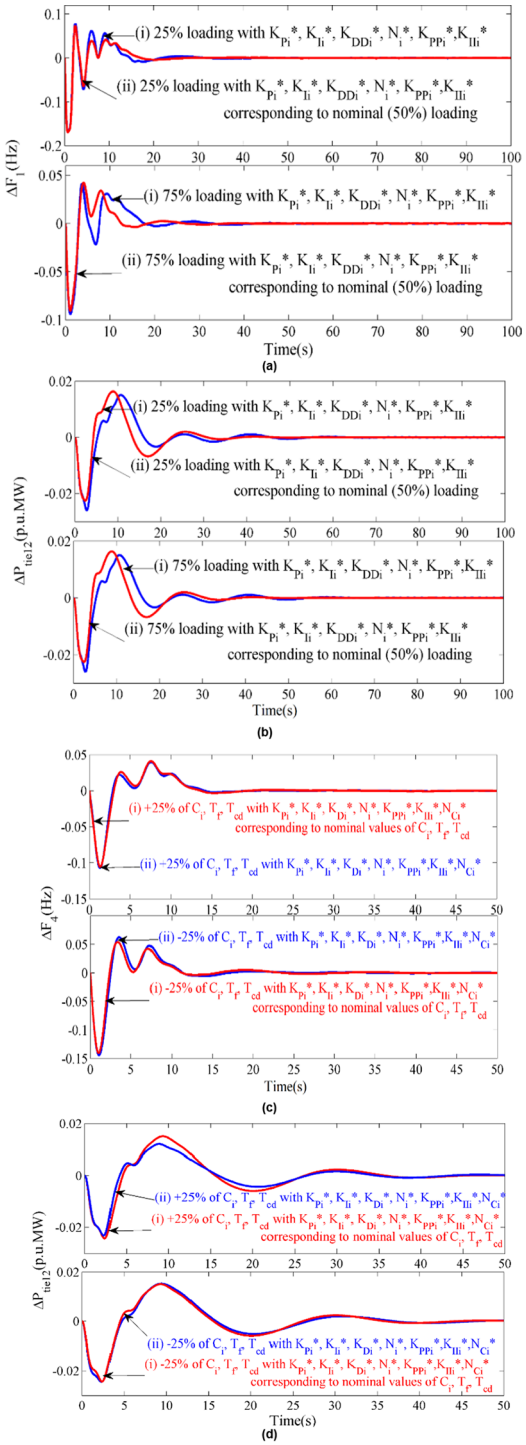

Fig. 7 Comparison of system dynamic responses during ± 25% change in system loading and gas generating unit parameters such as Ci, T_f and T_{cd} at the same time. **a** Frequency deviation in area 1 for ± 25% change in system loading. **b** Tie-power deviation in line connecting Area1 and 2 for ± 25% change in system loading. **c** Frequency deviation in Area 4 for ± 25% change in Ci, T_f and T_{cd} at the same time. **d** Tie-power deviation in line connecting Area 1 and 2 for ± 25% change in C_i, T_f and T at the same time

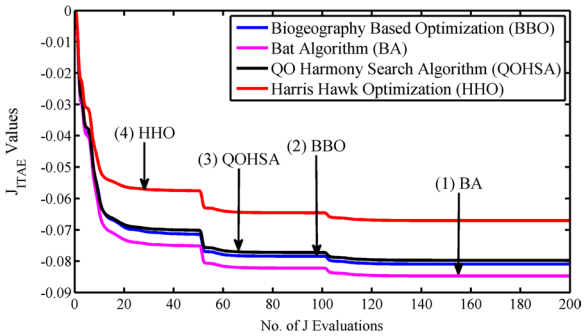

Fig. 8 Convergence characteristics of HHO with BA, QOHSA and BBO

Appendix

Parameter	Value
F, T_{gi}, T_{ri}, K_{ri}, T_{ti}	60 Hz, 0.08 s, 10 s, 0.5 s, 0.3 s
T_{cri}, T_{fi}, T_{cdi}, K_{gi}	0.3 s, 0.23 s, 0.2 s, 0.15
X_i, Y_i, b_i, C_i	0.6 s, 1 s, 0.05, 1
R_{AG} and R_i, T_{EVi}	2.4 Hz./p.u.MW, 1 s
T_{PS}, K_{PS}	20 s, 120 Hz./p.u.MW
H_i, T_w, D_i	5 s, 1.5 s, 0.00833 p.u.MW/Hz

Acknowledgements

Authors thank the Department of Electrical Engineering, Indian Institute of Engineering Science and Technology Shibpur, for providing necessary infrastructure to carry out the research work. Authors also thank the collaborating Institutes National Institute of Technology Silchar and Srinagar for their necessary non-financial support.

Author Information

Debdeep Saha is working in the Department of Electrical Engineering, Indian Institute of Engineering Science and Technology Shibpur, and has more than 10 years of teaching and research experience. His current research interests include Power System Operation and Control, Application of Soft Computing Techniques in Power Market, Energy Internet and Statistical Machine Learning. He has chaired several sessions in reputed International Conferences and has authored many publications.

Lalit Chandra Saikia is an Associate Professor in the Department of Electrical Engineering, National Institute of Technology Silchar, and has 24 years of teaching and research experience in the field of Power systems Control and Management. Dr. Saikia has done extensive research work in the broad area of Power System Control and Management, specifically on Automatic Generation Control in Conventional and Deregulated Power System, FACTS Devices and Applications of Artificial Intelligence Techniques in the field of Power System. He has published many research papers in International Journals and Conferences of repute.

Asadur Rahman is an Assistant Professor at Department of Electrical Engineering, National Institute of Technology Srinagar and has more than 10 years of experience of teaching and research. His research areas of interest are Power System Operations and Management, Restructuring and Deregulation of Power System, Solar Photovoltaic Systems, Renewable Energy, & Application of Intelligent Techniques in power system operations. He has published many research papers in reputed International Journals and Conferences of repute.

Author contributions
Conceptualization: DS and LCS. Methodology: DS and LCS. Validation: LCS and AR. Formal analysis: DS and LCS. Writing—original draft: DS. Writing—review and editing: DS, LCS and AR. Supervision: LCS and AR. All the authors read and approved the final manuscript.

Funding
This work is carried out without the support of any funding agency.

Availability of data and materials
Please contact author for data material request.

Declarations

Competing interests
The authors declare that they have no known competing financial interests or personal relationships that could have appeared to influence the work reported in this paper.

Author details
[1]Department of Electrical Engineering, Indian Institute of Engineering Science and Technology Shibpur, Shibpur, West Bengal, India. [2]Department of Electrical Engineering, National Institute of Technology Silchar, Silchar, Assam, India. [3]Department of Electrical Engineering, National Institute of Technology Srinagar, Srinagar, India.

Received: 23 September 2021 Accepted: 24 October 2022
Published online: 21 November 2022

References

1. Shankar, R., Pradhan, S. R., Chatterjee, K., & Mandal, R. (2017). A comprehensive state of the art literature survey on LFC mechanism for power system. *Renewable and Sustainable Energy Reviews., 76*, 1185–1207. https://doi.org/10.1016/j.rser.2017.02.064
2. Pandey, S. K., Mohanty, S. R., & Kishor, N. (2013). A literature survey on load–frequency control for conventional and distribution generation power systems. *Renewable and Sustainable Energy Reviews., 25*, 318–334. https://doi.org/10.1016/j.rser.2013.04.029
3. Fosha, C. E., Elgerd, O., & I,. (1970). The megawatt-frequency control problem: A new approach via optimal control theory. *IEEE Transaction on Power Apparatus and Systems, 89*(4), 563–577. https://doi.org/10.1109/TPAS.1970.292603
4. Cohn, N. (1956). Some aspects of tie-line bias control on interconnected power systems. *Transactions of the American Institute of Electrical Engineers Part III: Power Apparatus and Systems, 75*(3), 1415–1436. https://doi.org/10.1109/AIEEPAS.1956.4499454
5. Bevrani, H., & Hiyama, T. (2011). *Intelligent automatic generation control*. CRC Press.
6. Rahman, A., Saikia, L. C., & Sinha, N. (2015). Load frequency control of a hydro-thermal system under restructured environment using biogeography-based optimized three-degree-of-freedom integral-derivative controller. *IET Generation, Transmission & Distribution of Electri, 9*, 2284–2293. https://doi.org/10.1049/iet-gtd.2015.0317
7. Shiva, C. K., & Mukherjee, V. (2016). A novel quasi-oppositional harmony search algorithm for AGC optimization of three-area multi-unit power system after deregulation. *Engineering Science and Technology., 19*, 395–420. https://doi.org/10.1016/j.jestch.2015.07.013
8. Shiva, C. K., & Mukherjee, V. (2016). Design and analysis of multi-source multi-area restructured power system for automatic generation control using quasi-oppositional harmony search algorithm. *International Journal of Electrical Power & Energy Systems., 80*, 382–395. https://doi.org/10.1016/j.ijepes.2015.11.051
9. Morsali, J., Zare, K., & Mehrdad, T. H. (2017). Applying fractional order PID to design TCSC-based damping controller in coordination with automatic generation control of interconnected multi-source power system. *Engineering Science and Technology, an International Journal., 20*, 1–17. https://doi.org/10.1016/j.jestch.2016.06.002
10. Falahati, S., Taher, S., & Abbas, S. M. (2016). A new smart charging method for EVs for frequency control of smart grid. *International Journal of Electrical Power & Energy Systems., 83*, 458–469. https://doi.org/10.1016/j.ijepes.2016.04.039
11. Yingcheng, X., & Tai, N. (2011). Review of contribution to frequency control through variable speed wind turbine. *Renewable Energy, 36*, 1671–1677. https://doi.org/10.1016/j.renene.2010.11.009
12. Lee, D. J., & Wang, L. (2008). Small-signal stability analysis of an autonomous hybrid renewable energy power generation/energy storage system part I: Time-domain simulations. *IEEE Transactions on Energy Conversion., 23*, 311–320. https://doi.org/10.1109/TEC.2007.914309
13. Rahman, A., Saikia, L. C., & Sinha, N. (2017). Automatic generation control of an interconnected two-area hybrid thermal system considering dish-Stirling solar thermal and wind turbine system. *Renewable Energy, 105*, 41–54. https://doi.org/10.1016/j.renene.2016.12.048
14. Anderson, P. M., & Bose, A. (1983). Stability simulation of wind turbine systems. *IEEE Power Engineering Review., 3*(12), 3791–3795. https://doi.org/10.1109/TPAS.1983.317873
15. Nyugen, H., Zhang, C., & Apel, Md. M. (2014). Smart charging and discharging of electric vehicles to support grid with high penetration of renewable energy. *IFAC Proceedings., 47*, 8604–8609. https://doi.org/10.3182/20140824-6-ZA-1003.02109
16. Nguyen, N., & Mitra, J. (2016). An analysis of the effects and dependency of wind power penetration on system frequency regulation. *IEEE Transactions on Sustainable Energy., 7*, 354–363. https://doi.org/10.1109/TSTE.2015.2496970
17. Teng, F., Mu, Y., et al. (2016). Challenges of primary frequency control and benefits of primary frequency response support from electric vehicles. *Energy Procedia, 88*, 985–990. https://doi.org/10.1016/j.egypro.2016.06.123
18. Wu, L. & Infield, D. (2012). Investigation on the interaction between inertial response and droop control from variable speed wind turbines under changing wind conditions. In *47th International universities power engineering conference (UPEC)*, London, UK, pp. 1–6. https://doi.org/10.1109/UPEC.2012.6398429.
19. Wen, C. K., Chen, J. C., Teng, J. H., & Ting, P. (2012). Decentralized plug-in electric vehicle charging selection algorithm in power system. *IEEE Transactions on Smart Grid., 3*, 1779–1789. https://doi.org/10.1109/TSG.2012.2217761
20. Debbarma, S., & Dutta, A. (2017). Utilizing electric vehicles for LFC in power systems using fractional order controller. *IEEE Transactions on Smart Grid., 8*, 1–11. https://doi.org/10.1109/TSG.2016.2527821
21. Izadkhast, S., Garcia-Gonzalez, P., & Frías, P. (2016). An aggregate model of plug-in electric vehicles for primary frequency control. *IEEE Transactions on Power Systems., 30*, 1475–1482. https://doi.org/10.1109/TPWRS.2014.2337373
22. Liu, H., Hu, Z., Song, Y., Wang, J., & Xie, X. (2015). Vehicle-to-grid control for supplementary frequency regulation considering charging demands. *IEEE Transactions on Power Systems., 30*, 3110–3119. https://doi.org/10.1109/TPWRS.2014.2382979
23. Falahati, S., Taher, S. A., & Shahidehpour, M. (2016). Grid secondary frequency control by optimized fuzzy control of electric vehicles. *IEEE Transactions on Smart Grid, 99*, 1–10. https://doi.org/10.1109/TSG.2017.2692265
24. Singh, M., Kumar, P., & Karl, M. (2012). Implementation of vehicle to grid infrastructure using fuzzy logic controller. *IEEE Transactions on Smart Grid, 3*, 565–577. https://doi.org/10.1109/TSG.2011.2172697
25. Johnson, M. A., & Moradi Md, H. (2005). *New identification and design*. Springer.
26. Jeng, J. C., & Liao, S. J. (2013). A simultaneous tuning method for cascade control systems based on direct use of plant data. *Industrial & Engineering Chemistry Research., 52*(47), 16820–16831. https://doi.org/10.1021/ie401978p
27. Dash, P., Saikia, L. C., & Sinha, N. (2016). Flower pollination algorithm optimized PI-PD cascade controller in automatic generation control of a multi-area power system. *International Journal of Electrical Power & Energy Systems., 82*, 19–28. https://doi.org/10.1016/j.ijepes.2016.02.028
28. Dash, P., Saikia, L. C., & Sinha, N. (2015). Automatic generation control of multi area thermal system using Bat algorithm optimized PD–PID

cascade controller. *International Journal of Elect Power & Energy Systems, 68*, 364–372. https://doi.org/10.1016/j.ijepes.2014.12.063
29. Asghar, H. A., Seyedali, M., Hossam, F., Ibrahim, A., Majdi, M., & Huiling, C. (2019). Harris hawks optimization: Algorithm and applications. *Future Generation Computer Systems, 97*, 849–872. https://doi.org/10.1016/j.future.2019.02.028
30. Abubakr, H., Hassan, M. T., Hussein Mahmoud, M., Guerrero, J. M., & Gibran, A.-T. (2021). Adaptive frequency regulation strategy in multi-area microgrids including renewable energy and electric vehicles supported by virtual inertia. *International Journal of Electrical Power & Energy Systems, 129*, 106814. https://doi.org/10.1016/j.ijepes.2021.106814
31. Abd, E. M., Asghar, H. A., Hamido, F., & Hossein, M. (2020). A competitive chain-based Harris Hawks Optimizer for global optimization and multi-level image thresholding problems. *Applied Soft Computing, 95*, 106347. https://doi.org/10.1016/j.asoc.2020.106347
32. Dillip, K., Kumar, S. R., Sekhar, G. T., & Sidhartha, P. (2020). Automatic generation control of power system in restructured environment using hybrid TLBO and pattern search technique. *Ain Shams Engineering Journal, 11*, 553–573. https://doi.org/10.1016/j.asej.2019.10.012
33. Ghasemi-Marzbali, A. (2020). Multi-area multi-source automatic generation control in deregulated power system. *Energy, 201*, 117667. https://doi.org/10.1016/j.energy.2020.117667
34. Musa, K., Haishun, S., Yingmeng, X., & Di, S. (2021). Electric vehicles participation in load frequency control based on mixed H_2/H_∞. *Electrical Power and Energy Systems, 125*, 106420. https://doi.org/10.1016/j.ijepes.2020.106420